Stress analysis and fracture simulation of aluminosilicate glass plates under Ring-On-Ring loading

Zhen Wang [a,b,*], Andrea Manes [b]

[a] School of Aeronautics, Northwestern Polytechnical University, Xi'an, Shaanxi 710072, China
[b] Politecnico di Milano, Department of Mechanical Engineering, Milan 20156, Italy

ABSTRACT

Ring-On-Ring (ROR) tests have been widely applied to evaluate the biaxial flexural strength of brittle materials. Properly designed geometry of specimens and loading configurations are essential for accurate test results. In this paper, the stress distribution of round glass plates subjected to loading between concentric rings was investigated via finite element analysis. In particular, the effects of the ratio of the ring diameter, overhang and thickness of plates were studied and discussed. ROR tests on aluminosilicate glass were then conducted together with numerical simulations based on the smeared fixed crack method. The out-of-plane deformation of glass plates can be reproduced well by the numerical model. In order to mimic the observed fracture modes, numerical models with different mesh geometries were utilized and compared. Unstructured quadrilateral mesh and triangular mesh types were proven to be efficient in reproducing the fracture and failure morphology of glass specimens.

1. Introduction

The increased demand of glass products has created great opportunities for designing strong and lightweight transparent structures. Aluminosilicate glass is one kind of inorganic glass widely used in military vehicles, airplanes and electronic devices. However, the correct design of the glass components and structures is not straightforward. The strength of brittle materials such as glass and ceramics is a function of the specimen size and the state of applied stress [1,2], making it difficult to evaluate the safety of such brittle components. Glass structures are often subject to multiaxial stresses during service and hence, in order to assess the strength of such components, specific test methods are required. The Ring-On-Ring (ROR) test is a typical test method to measure the strength of brittle materials under biaxial flexural loading; and this test method has been standardized in ASTM C1499 [3]. The test configuration consists of a pair of concentrate rings: the outer one is used as the support for the disk sample and the inner ring is used to apply an increasing load. Both rings have rounded edges to minimize local stress concentrations. As for bar shape specimens used for uniaxial flexural tests such as three-point bending and four-point bending, the strength of glass specimens is sometimes sensitive to the machining and processing of the specimens, which can lead to chips and defects along the edges and decrease the measured strength. For disk specimens used in ROR

tests, the specimen is highly stressed within the inner ring area and the stresses developed are lowest at the edges, thereby minimizing spurious failure. ROR tests on glass [4], ceramic [5], concrete [6] and composite plates [7] have been reported in literature. However, detailed stress analysis of disk specimens considering the effect of loading configuration and specimen geometry is still necessary for a better understanding of this test method.

As for numerical simulations, finite element method (FEM) is an efficient tool for deformation and stress analysis of engineering structures even if the presence of discontinuity like cracks pose some modeling challenges, especially if these are widely present in the material. In brittle materials, crack initiation and propagation usually happen when the failure strength is reached and several approaches have been developed to describe cracks in solid materials. Element deletion can be assigned to the elements reaching the failure criteria. [8] This method is very simple and widely used to avoid element distortion problems. However, deleting elements directly from the numerical model is a non-physical process violating the conservation of mass and energy. Also, considering a brittle solid material containing one single crack, it can still bear a compressive load perpendicular to the crack surface. It is hard to mimic such a crack closure effect via an element erosion method. A coupled FEM and smoothed particle hydrodynamics (SPH) method has been developed and is used in fracture problems of

* Corresponding author.
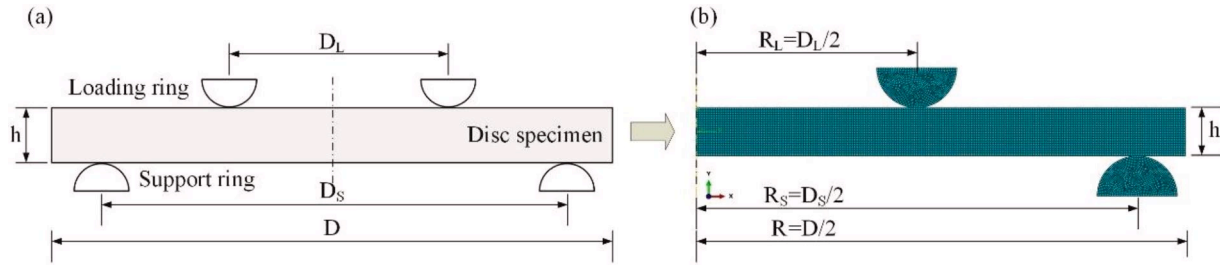 *E-mail address:* zhen.wang@polimi.it (Z. Wang).

Fig. 1. (a) Schematic of ROR test; (b) axisymmetric finite element model.

ceramics [9], glass [10] and rock [11], in which eroded elements are replaced by SPH particles inheriting the mass and energy of solid elements. The cohesive zone method is also a very popular method for brittle material simulations. [12,13] Zero-thickness cohesive elements can be inserted into every two solid elements to represent the potential cracks. These cohesive elements obey the traction-separation law and will be deleted once the failure criteria are met. Recently, some meshless methods have also been developed for brittle fracture simulations, such as the discrete element method (DEM) [14] and the element-free Galerkin method (EFG) [15]. However, when meshless methods or cohesive element method are used, their calculation efficiency is still much lower than the FEM efficiency [10]. For large engineering structures, an extremely high number of cohesive elements or particles should be used, taking up both a lot of time and computing resources. This limits the further applications of meshless methods in the analysis of engineering structures. Another approach for fracture simulation of brittle materials is the smeared fixed crack model in the FEM. [16,17] This method accounts for the effect of a crack by the reduction or even the elimination of the elastic stiffness of the element. Two perpendicular cracks can be defined in one element and the cracks can open and close independently, which can describe the fracture behavior of brittle materials accurately. Before the cracks initiate in the elements, the simple linear elastic deformation is defined for the elements, which can save computational costs compared to other numerical methods. Also, this method can be used in shell elements, which is more efficient and can be easily used in large thin-walled structures.

In this paper, the stress analysis of plate specimens under ROR loading was conducted and is presented in section 2 via FEM simulations in order to investigate the effect of loading configurations on the validity of ROR tests. In particular, the effects of the ratio of the ring diameter, overhang and thickness of glass plates were studied and discussed. Section 3 describes the experimental tests conducted on aluminosilicate glass with the aid of 3D-DIC technique. In section 4, in order to analyze the fracture mechanism and replicate the precise fracture modes of glass

plates, the smeared fixed crack method was used for the deformation and fracture simulation of glass plates and the numerical results were compared with experimental data in detail. Finally, section 5 provides the main conclusions of this work.

2. Stress analysis of glass plates subjected to ROR loading

2.1. Stress distribution of the plate specimen

A schematic of the ROR test is shown in Fig. 1(a). The theoretical solution for the deflection at the center point of the plate can be expressed as [18]

$$w = \frac{3P(1-\mu^2)R_L^2}{2\pi Eh^3}\left[\frac{R_s^2}{R_L^2} + \frac{R_s^2(1-\mu)\left(R_s^2 - R_L^2\right)}{2(1+\mu)R^2R_L^2} - ln\left(\frac{R_L^2}{R_s^2}\right) - 1\right] \quad (1)$$

where P is the applied peak load, E and μ are the Young's modulus and Poisson's ratio of the plate's material. R, R_s, R_L and h represent the radius of the specimen, the radius of support ring, the radius of loading ring and the thickness of specimen respectively, as shown in Fig. 1. The biaxial flexural strength of ROR specimens can be calculated by [19]

$$\sigma_{ROR} = \frac{3P}{2\pi h^2}\left[(1-\mu)\frac{R_s^2 - R_L^2}{2R^2} + (1+\mu)ln\frac{R_s}{R_L}\right] \quad (2)$$

The test was originally designed for small deflections (less than one-fourth of the specimen's thickness) using linear equations [20]. Thus, the specimen's thickness shouldn't be too thin to restrict the use of linear geometric relations.

In order to obtain the typical stress distribution properties of ROR specimens, an axisymmetric 2D FEM was built, as shown in Fig. 1(b). The size of the numerical specimen is the same as the real glass sample introduced in the following section, where $R = 61$ mm, $t = 6$ mm. The radius of the support ring was 55 mm and the radius of loading ring R_L was set as half of R_s in this simulation. A linear elastic material property
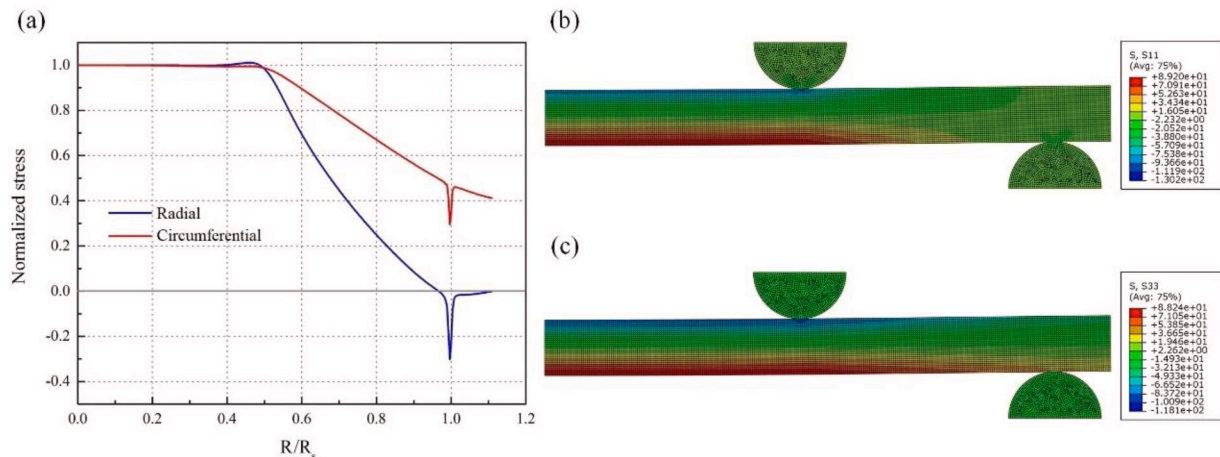

Fig. 2. (a) Normalized stress at the glass tensile surface; (b) radial stress field; (c) circumferential stress field.

Table 1
Parameters for different loading configurations.

h (mm)	D_L (mm)	D (mm)
6	33	116/122/134/146/158
6	44	116/122/134/146/158
6	55	116/122/134/146/158
8	55	118/126/142/158/174
10	55	120/130/150/170/190

was assigned to the model with an elastic modulus of 75 GPa and a Poisson's ratio of 0.22 for aluminosilicate glass [21]. The friction coefficient between the plate and rings was set as 0.05 [1]. A fine mesh size of 0.2 mm with 9150 4-node quadrilateral shell elements for the numerical specimen was used to obtain accurate stress distribution results. Mesh size sensitivity analysis was conducted and this mesh size was proven to provide accurate stress distributions. For the boundary condition, the support ring was fixed and the loading ring was given a vertical displacement of 0.3 mm to load the specimen. This displacement is much lower than the specimen's thickness, so there is no need to consider the geometric non-linearities in this study [22]. All subsequent analyses in this paper were performed in the range of the linear plate theory.

The radial and circumferential stress at the lower surface of the plate specimen along the radius direction is shown in Fig. 2(a). It should be noted that the stress was normalized by the stress value at the center of the specimen for convenience. The radial and circumferential stress nephograms on the cross section of the specimen are provided in Fig. 2 (b) and (c) respectively. Both the radial and circumferential stress on the tensile surface is maximum and nearly constant inside the loading ring area and decreases out of the loading ring area. The normalized radial stress at the loading ring contact area (R/R_S=0.5) is a little higher than 1, which is actually not expected during tests and this difference should be minimized. Theoretically, the stress distribution in the loading ring area of the ROR specimens is regarded as uniform and this constant stress can be calculated by Eq. (1). In a real loading condition, if this stress distribution is not uniform, the precision for the biaxial flexural strength calculation will be challenged. Sudden changes in the curves when R/R_S=1 are visible. These changes are caused by the contact of the bottom elements in the numerical specimen with the support ring and won't influence the final results. The radial stress around the edge of the plate is zero, however, the circumferential stress is not zero at the edge and should be considered during the tests. As there are always defects and chips present around the edge of glass plates occurring during the manufacturing process, these defects can be more severe than those inherent on the surface of the disk. As a result, failure of the plate may occur at the edge instead of inside of the loading ring as expected. In that case the measured biaxial strength should be lower than its real value. In order to ensure that the plates ultimately fail from the inside of the loading ring, the specimens should be designed so that the edge stresses are minimized.

2.2. Parameter study

In order to investigate the effect of loading configurations and specimen's geometry on the stress distribution of disk specimens, a series of numerical models were built and simulated. The diameter of the support ring D_S was kept constant as 110 mm, but the loading ring diameter D_L, the specimen's diameter D and the thickness h differed, as shown in Table 1. A total of 25 numerical models were utilized here to study the effect of the ratio of the ring diameter, overhang, and thickness of plates via a variable-controlling approach. The ratio of the ring diameter was defined as D_L/D_S, corresponding to 0.3, 0.4 and 0.5 when D_L is equal to 33 mm, 44 mm and 55 mm. In order to study the effect of the overhang, the parameter $(D-D_S)/2h$ was defined to represent different overhang conditions. A higher value of $(D-D_S)/2h$ means a
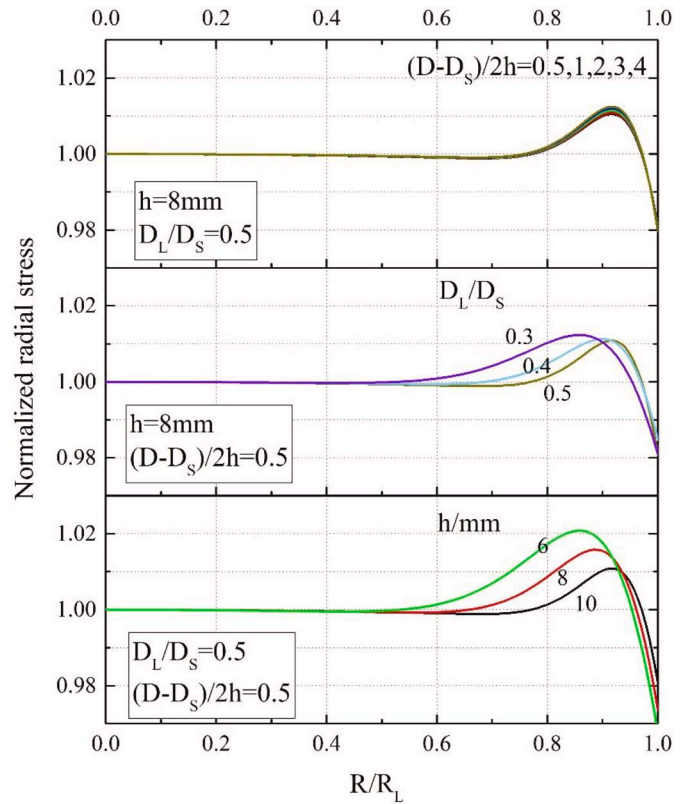

Fig. 3. Normalized radial stress as a function of overhang, ring diameter ratio and plate thickness.
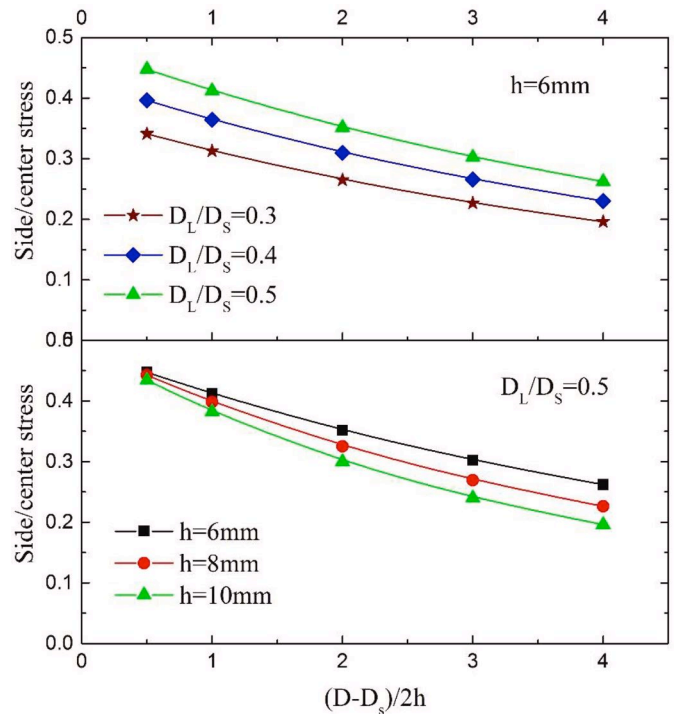

Fig. 4. Ratio of the edge to center stress as a function of overhang, ring diameter ratio and plate thickness.

larger overhang of the glass plates. Here, $(D-D_S)/2$ h is equal to 0.5, 1, 2, 3, 4 with different values of D and h. For the effect of specimen thickness, different values of 6 mm, 8 mm and 10 mm were used.
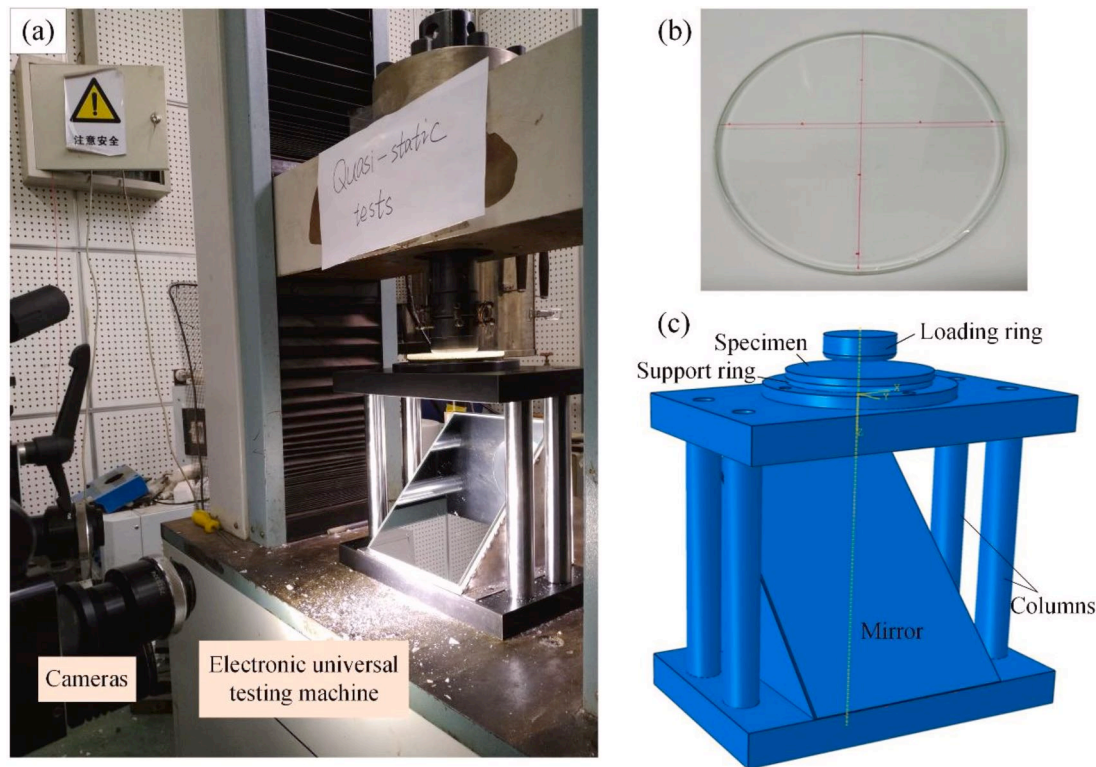
Fig. 5. (a) Experimental set-ups for ROR tests; (b) glass specimen; (c) specially designed loading fixture with a 45° mirror for 3D-DIC measurement.

Fig. 3 shows the effect of the overhang, ring diameter ratio and specimen thickness on the radial stress distribution inside the loading ring area. For each parameter studied, the other two parameters were kept constant for convenience of comparison. At or near the center of the plate, the stress is equal to its theoretical value. Inside the loading ring, the stress is slightly higher. It can be seen that the overhang has little effect on the radial stress distribution. With the increase of the ring diameter ratio and specimen thickness, the stress distribution is more uniform. However, it should be noted that even for the "worst" conditions studied, the radial stress around the loading ring on the plate is only 2% larger than the radial stress in the center, which is acceptable during tests.

The effect of the overhang, ring diameter ratio and plate thickness on the edge stress is shown in Fig. 4. The y-axis is set as the ratio of the edge circumferential stress and center stress and a smaller value for this parameter is always expected to avoid edge fracture during tests. It can be clearly seen that as the degree of the overhang increases the circumferential stress at the edge decreases. Furthermore, the edge stress decreases with the decrease of the ring diameter ratio. When $(D-D_S)/2h$=0.5, the effect of the plate thickness is minimized. With the increase of the degree of overhang, the edge stress of thin plates is much higher than of thick plates. Thus, a thick plate specimen with a large overhang and a small ring diameter ratio is helpful to decrease the edge stress of the specimen.

3. Experimental procedure

A universal electronic testing machine was utilized to load the glass plates at a constant loading speed of 0.2 mm/min, which can be regarded as a quasi-static loading condition, as shown in Fig. 5. The specimens produced from 6 mm thick aluminosilicate glass plates are disk samples with a diameter of 122 mm. The diameters of the loading ring and support ring were 50 mm and 110 mm respectively. A special designed loading fixture with a 45° mirror was used here for convenience of deformation measurement via a three-dimensional digital

image correlation (3D-DIC) technique. During the experiments, random paint spots were sprayed onto the bottom surface of the glass specimens. These spots are reflected by the mirror and were captured by the two synchronous shooting cameras. Then the out-of-plane displacement of the disk specimen were calculated based on the professional DIC software. Detailed information about this experimental technique was presented in our previous work [23].

4. Finite element analysis

4.1. Smeared fixed crack method

The material model used in this study to represent the fracture and failure behavior of glass is the smeared fixed crack model, which was initially introduced by Hillerborg et al. [24] for concrete. This model uses the cohesive zone concept and was implemented in LS-DYNA as MAT280_Glass. Only shell elements can be used for this model at present and there have to be sufficient integration points distributed over the thickness of the shell elements to represent the gradient stress distribution over the thickness direction. The default value of NIPF=1 (number of failed through thickness integration points needed to fail all through thickness integration points) resembles the fact, that a crack in a glass plate immediately runs through the thickness. The term "smeared crack" denotes that the model does not represent a micro-crack explicitly, but instead the model accounts for the effect of a crack by an elastic stiffness reduction, or even elimination, at the integration points of an element. [16] The underlying material behavior before failure is isotropic, small strain linear elasticity with Young's modulus, E, and Poisson's ratio, v. Asymmetric (tension-compression dependent) failure happens as soon as one of the following plane stress failure criteria is reached.
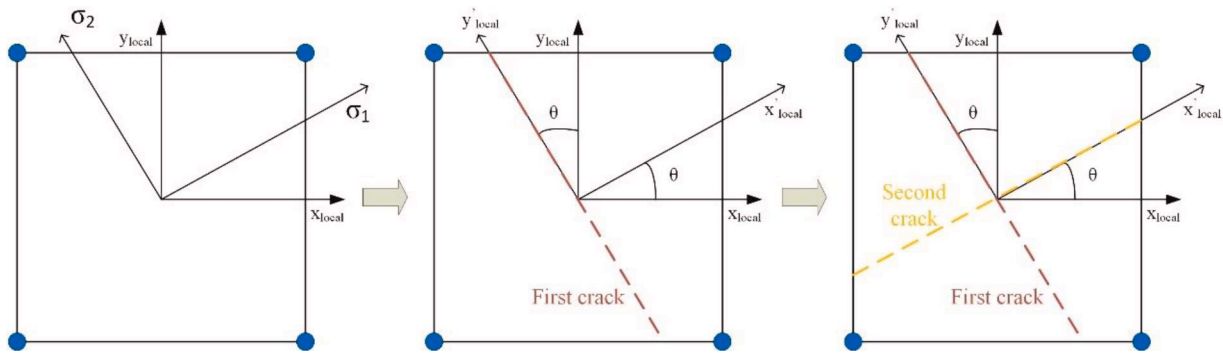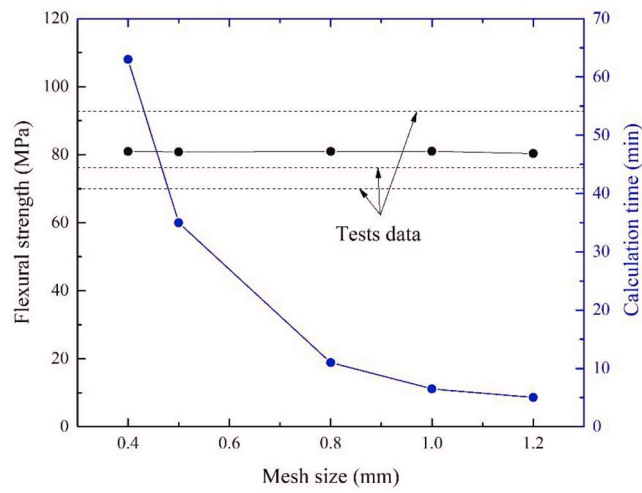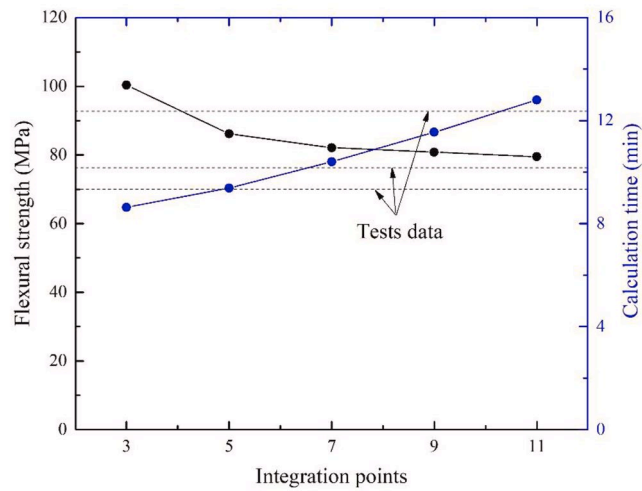
Fig. 6. Failure process of one single element which can contain two orthogonal cracks.
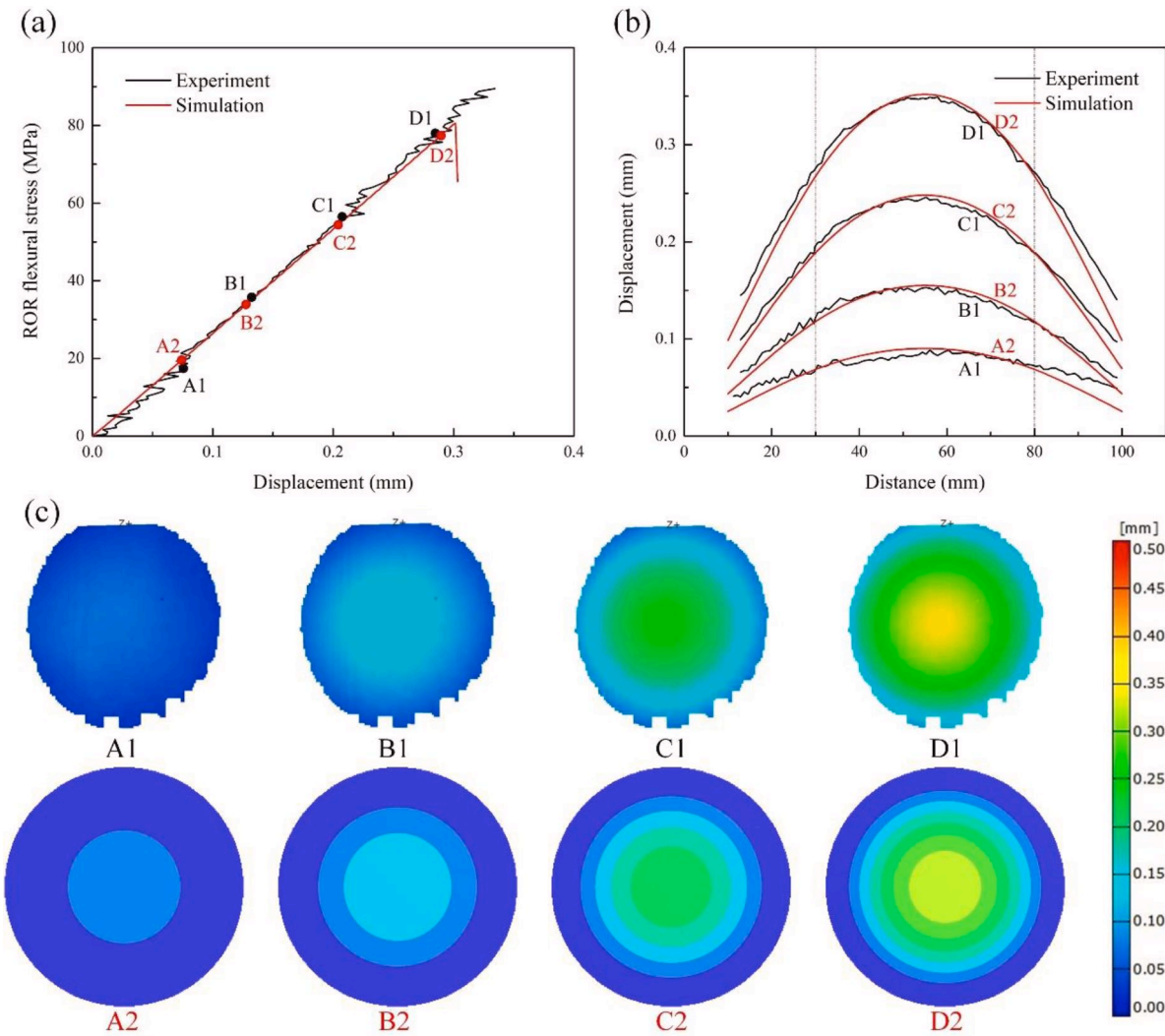

(a) Effect of mesh size on the simulated biaxial flexural strength and calculation time

(b) Effect of integration points on the simulated biaxial flexural strength and calculation time

Fig. 7. Simulation parameters calibration.

Fig. 8. Comparison between ROR test and simulation. (a) Flexural stress-displacement curve; (b) out-of-plane displacement at different stages; (c) full-field out-of-plane displacement from DIC and simulation.

$$
\begin{cases}
\max\left(\dfrac{\sigma_1}{FT}, \dfrac{\sigma_2}{FT}\right)\Big\langle 1 & \text{if } \sigma_1 > 0 \text{ and } \sigma_2 > 0 \\[2mm]
\max\left(-\dfrac{\sigma_1}{FC}, -\dfrac{\sigma_2}{FC}\right)\Big\langle 1 & \text{if } \sigma_1 < 0 \text{ and } \sigma_2 < 0 \\[2mm]
\dfrac{\sigma_1}{FT} - \dfrac{\sigma_2}{FC} < 1 & \text{if } \sigma_1 > 0 \text{ and } \sigma_2 < 0 \\[2mm]
-\dfrac{\sigma_1}{FT} + \dfrac{\sigma_2}{FC} < 1 & \text{if } \sigma_1 < 0 \text{ and } \sigma_2 > 0
\end{cases}
\tag{3}
$$

where principal stresses σ_1 and σ_2 are bounded by the defined tensile strength FT and compression strength FC. This failure criteria is also called the Mohr-Coulomb failure criteria [25]. As soon as failure happens in the tensile regime, a crack occurs perpendicular to the maximum principal stress direction, as shown in Fig. 6. The element can no longer carry any tensile load in that direction but can still bear compression loads due to the crack closure effect defined in this method. This damaged element can also carry loads parallel to the first crack and a second crack can occur, orthogonal to the first crack. These load carrying properties correspond very well with the mechanical properties of silicate glass. In our model, shell elements were used for simulation (ELFORM=2). Once the failure criteria of one element was reached, the element were not deleted but appropriate stress and stiffness tensor components (e.g., normal to the crack) were reduced to a defined small

value. In this study, the material stiffness was reduced to 0.1% in case of failure within 10 time-step cycles (SFSTI=0.001, NCYCR=10). After that, a second crack orthogonal to the first crack could occur which could open and close independently from the first one, thus further reducing the element stiffness, as illustrated in Fig. 6. The strength data obtained from ROR tests are set as FT in the numerical simulations, while the quasi-static compression strength 600 MPa of aluminosilicate glass is used for FC. It should be mentioned that this numerical method is very suitable for multi-axial loading conditions with the definition of orthogonal cracks.

4.2. Effect of mesh size and integration points on flexural strength

In order to investigate the effect of mesh size and number of integration points on the simulation results, different models were built and compared. A powerful personal computer (CPU AMD Ryzen 9–3900X, 3.79 GHz, 12 cores / 24 threads, 64 GB RAM) was employed for all the simulations and the calculation efficiency of different models was also compared. The dashed lines in Fig. 7 represents the experimental data. Fig. 7(a) shows the absence of an no apparent mesh size dependence at the simulated mesh size range (0.4 mm – 1.2 mm). With the decrease of mesh size, the number of elements increased remarkably, together with the calculation time. Fig. 7(b) shows the relationship between flexural strength / calculation time and integration points. With the increase of
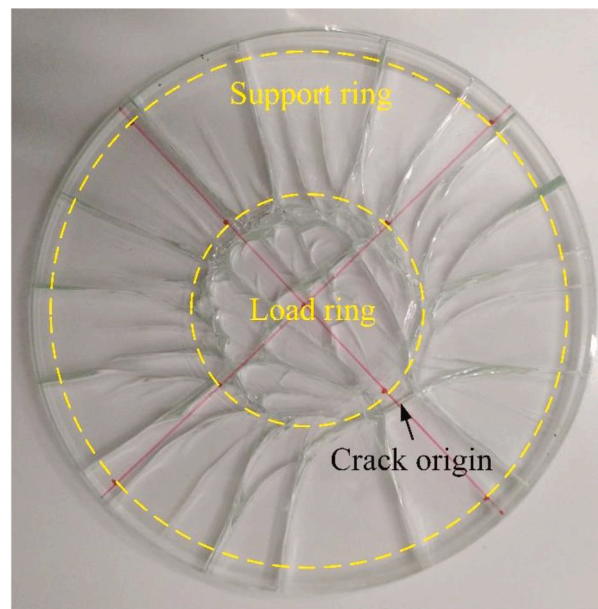
(a) Typical fracture model of glass specimen under ROR loading
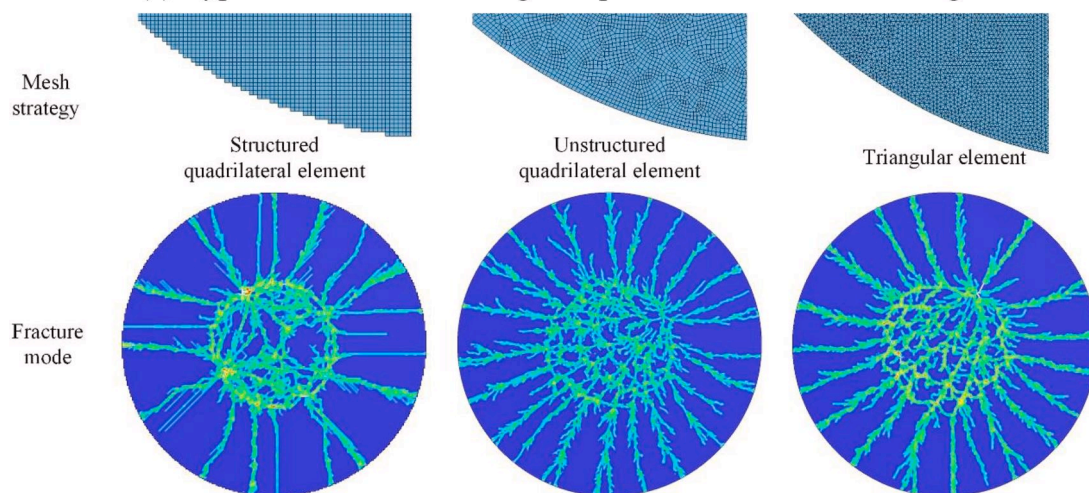
(b) Fracture mode simulation on glass specimens with different mesh types.

Fig. 9. Comparison of the fracture mode between experimental observations and numerical simulations with different mesh strategies.

integration points along the thickness direction of the shell elements, the simulated flexural strength decreased and finally became stable. The stable value is comparable to experimental results from ROR tests. The reason for this trend is that the integration points are far from the surface of the glass tile when less integration points are used, leading to the overestimation of the strength data. Also, with the increase of integration points, the calculation time increased. In order to balance the calculation efficiency and accuracy, nine integration points and the mesh size of 0.8 mm were used for the following simulations in this work.

4.3. Deformation field analysis

The detailed out-of-plane displacement field of the plate specimens can be obtained from the 3D-DIC set-up described in section 3. The comparison between the test and simulation results is shown in Fig. 8. The simulated flexural stress – displacement curve is linear elastic and comparable to the experimental curve. The deformation field of the specimens at different stages during the loading process is also provided and is fully comparable to the experimental results. It is illustrated that

the proposed numerical model is able to mimic both the deformation field and failure strength of the ROR specimens.

4.4. Fracture mode analysis

The typical fracture mode of aluminosilicate glass specimen under ROR loading is shown in Fig. 9(a). The fracture origin is located around the inner ring area, which is a very important feature to identify the effectiveness of this test [26]. For the ROR specimen the crack originates from a pair of branches in the opposite directions. Following the occurrence of the first break, the larger remnant may still bear load from the inner loading ring, and the inner part of the remnant in turn breaks in bending, consistent with the fact that glass containing a single crack can still carry load parallel to this crack. Thus, cross cracks formed in the inner ring area. The stress distribution outside of the inner ring was mainly circumferential stress perpendicular to the radius direction and radial cracks were driven in this region.

The simulation results are provided in Fig. 9(b). Three different mesh strategies, including structured quadrilateral mesh, unstructured quadrilateral mesh and triangular mesh were utilized for this simulation. The
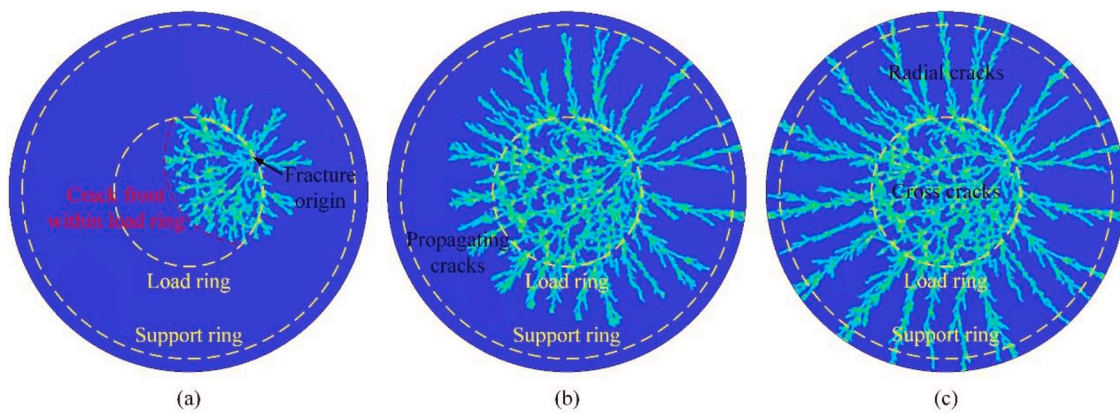
Fig. 10. Simulated failure process and fracture patterns of glass plate under ROR biaxial flexural loading.
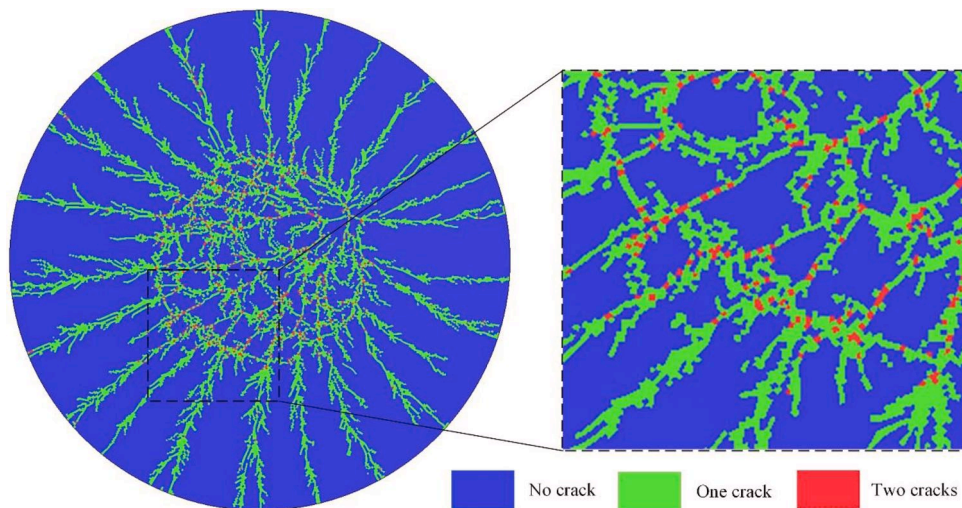

Fig. 11. Crack pattern analysis for the shell elements in the smeared fixed crack method simulation.

basic fracture mode of glass specimen shown in Fig. 9(a) was reproduced by all three models. However, a similar crack branching and propagation route as observed in the experiments was reproduced via the unstructured quadrilateral mesh and the triangular mesh models mainly due to the randomly distributed element shapes and directions, while the smeared fixed crack method was very efficient for biaxial flexural simulations.

As the fracture process of glass is very fast and usually timed in several microseconds, ultra-high-speed cameras are essential to record the fracture images. However, the fracture sequence of the numerical specimen is easy to be obtained by defining a proper data output frequency in the numerical model, as shown in Fig. 10. It can be seen in Fig. 10(a) that the fracture initiates around the inner load ring and propagates outwards quickly. Within the load ring, the cracks form a radial-emitting crack front from the fracture origin, illustrated as the red dashed line, in consistence with the observations of dynamic fracturing of strengthened glass reported in [27]. In the next frame (Fig. 10(b)), the crack front propagates further away from the origin to release more stored elastic energy. The radial cracks emitting from the fracture origin intersect with the load ring induced circumferential cracks. Within the loading ring, the crack saturates. In the last frame shown in Fig. 10(c), cross cracks form in the inner ring area and radial cracks form in the outer area due to different stress distributions in different areas.

As introduced in section 4.1, the smeared fixed crack model can represent at most two independent orthogonal cracks in one single element. In order to further illustrate the crack patterns in simulation,

the "history variable 1″ for crack flag in LS-DYNA can be introduced, as shown in Fig. 11. This is the simulation result by the unstructured quadrilateral mesh model and different colors represent different crack modes for the elements. It should be noted that all the cracks were formed due to tensile fracture in this study because the compression strength of aluminosilicate glass is one order higher than its tensile strength. Most of the radial cracks only contain one tensile crack, as the stress distribution outside of the inner ring is mainly circumferential stress perpendicular to the radius direction. In the inner ring area, some elements contain two cracks, especially at the intersection region of the cracks. This means that the multiaxial fracture behavior of aluminosilicate glass can be efficiently reproduced by this numerical method.

5. Conclusions

ROR test generates an equibiaxial stress state for the plate specimen inside the loading ring. The stress distribution of an aluminosilicate glass plate under ROR loading is simulated and analyzed in detail. It is illustrated that the overhang of the specimen has little effect on the radial stress distribution. With the increase of the ring diameter ratio and specimen thickness, the stress distribution is more uniform. In order to avoid edge fracture of the glass specimens, a low edge stress is always expected during tests. It is illustrated from the numerical simulations that the choice of a thick plate specimen with a large overhang and smaller ring diameter ratio is helpful to decrease the edge stress of the specimen.

ROR tests and corresponding simulations were then conducted and compared. The proposed numerical model is based on the smeared fixed crack method. This numerical method can consider both the crack closure effect and orthogonal cracks in one element, which is very suitable for fracture simulation of glass. The proposed model is able to mimic both the deformation field and failure strength of ROR specimens. In order to replicate the precise fracture modes of glass plates, numerical models with unstructured quadrilateral and triangular meshes are preferential due to the heterogeneous element distributions.

Declaration of Competing Interest

The authors declare no conflict of interest.

Acknowledgment

References

[1] L.M. Powers, J.A. Salem, A.S. Weaver, Stresses in ceramic plates subjected to loading between concentric rings, ASTM Spec. Tech. Publ. (2002) 30–45, https://doi.org/10.1520/stp10470s.

[2] J.J. Swab, P.J. Patel, X. Tran, L. Gilde, E. Luoto, M.H. Gaviola, et al., Equibiaxial flexure strength of glass: influence of glass plate size and equibiaxial ring ratio, Int. J. Appl. Glas. Sci. 5 (2014) 384–392.

[3] A. Standard, Standard test method for monotonic equibiaxial flexural strength of advanced ceramics at ambient temperature, Stand. ASTM C1499-04 (2005). West Conshohocken.

[4] I. Mohagheghian, Y. Wang, L. Jiang, X. Zhang, X. Guo, Y. Yan, et al., Quasi-static bending and low velocity impact performance of monolithic and laminated glass windows employing chemically strengthened glass, Eur. J. Mech. 63 (2017) 165–186.

[5] S. Kondo, Y. Katoh, L.L. Snead, Concentric ring on ring test for unirradiated and irradiated miniature SiC specimens, J. Nucl. Mater. 417 (2011) 406–410.

[6] J. Kim, D.J. Kim, G. Zi, Improvement of the biaxial flexure test method for concrete, Cem. Concr. Compos. 37 (2013) 154–160, https://doi.org/10.1016/J.CEMCONCOMP.2012.11.001.

[7] D. Deland, Z. Zhang, K. Kirane, Biaxial flexural failure of woven composite plates investigated by the ring on ring bending test, Thin-Walled Struct. 148 (2020), 106585.

[8] J. Pelfrene, S. Van Dam, R. Sevenois, F. Gilabert, W. Van Paepegem, Fracture simulation of structural glass by element deletion in explicit FEM, Challeng. Glas. Conf. Proc. 5 (2016) 439–454, vol.

[9] R. Scazzosi, M. Giglio, A. Manes, FE coupled to SPH numerical model for the simulation of high-velocity impact on ceramic based ballistic shields, Ceram. Int. (2020).

[10] Z. Wang, D. Ma, T. Suo, Y. Li, A. Manes, Investigation into different numerical methods in predicting the response of aluminosilicate glass under quasi-static and impact loading conditions, Int. J. Mech. Sci. 196 (2021), https://doi.org/10.1016/j.ijmecsci.2021.106286.

[11] A. Mardalizad, T. Saksala, A. Manes, M. Giglio, Numerical modeling of the tool-rock penetration process using FEM coupled with SPH technique, J. Pet. Sci. Eng. 189 (2020), 107008.

[12] Z. Wang, J. Fu, A. Manes, Discrete fracture and size effect of aluminosilicate glass under flexural loading: monte Carlo simulations and experimental validation, Theor. Appl. Fract. Mech. 111 (2021), 102864.

[13] M. Vocialta, M. Corrado, J.F. Molinari, Numerical analysis of fragmentation in tempered glass with parallel dynamic insertion of cohesive elements, Eng. Fract. Mech. 188 (2018) 448–469, https://doi.org/10.1016/j.engfracmech.2017.09.015.

[14] Z. You, M. Zhang, F. Liu, Y. Ma, Numerical investigation of the tensile strength of loess using discrete element method, Eng. Fract. Mech. 247 (2021), 107610, https://doi.org/10.1016/j.engfracmech.2021.107610.

[15] D. Ma, A. Esmaeili, A. Manes, C. Sbarufatti, A. Jiménez-Suárez, M. Giglio, et al., Numerical study of static and dynamic fracture behaviours of neat epoxy resin, Mech. Mater. 140 (2020), 103214.

[16] M.J. Meyland, J.H. Nielsen, Ongoing research into the failure of glass at high strain-rates, Challeng. Glas. Conf. Proc. 7 (2020).

[17] A. Rimkus, V. Cervenka, V. Gribniak, J. Cervenka, Uncertainty of the smeared crack model applied to RC beams, Eng. Fract. Mech. 233 (2020), 107088, https://doi.org/10.1016/J.ENGFRACMECH.2020.107088.

[18] F.F. Vitman, V.P. Pukh, A method for determining the strength of sheet glass, Ind. Lab. 29 (1963) 925–930.

[19] S.W. Freiman, J.J. Mecholsky Jr, The Fracture of Brittle Materials: Testing and Analysis, John Wiley \& Sons, 2019.

[20] K.H. Vepakomma, J. Westbrook, S. Carley, J Kim, Finite element analysis of Ring-on-Ring test on LCD panels, J. Disp. Technol. 9 (2013) 673–677.

[21] M.Z. Sheikh, W. Zhen, S. Tao, L. Yulong, Z. Fenghua, A. Majeed, et al., Dynamic failure of un-strengthened aluminosilicate glass, Theor. Appl. Fract. Mech. 104 (2019), 102325.

[22] G. Castori, G. Pisano, E. Speranzini, A theoretically-based novel protocol for the analytic treatment of the glass failure stresses associated with coaxial double ring test method, Ceram. Int. 47 (2021) 19784–19799, https://doi.org/10.1016/J.CERAMINT.2021.03.318.

[23] Z. Wang, T. Ren, T. Suo, A. Manes, Quasi-static and low-velocity impact biaxial flexural fracture of aluminosilicate glass — an experimental and numerical study, Thin-Walled Struct. 165 (2021), 107939, https://doi.org/10.1016/j.tws.2021.107939.

[24] Hillerborg A., Modéer M., Petersson P.E. Analysis of crack formation and crack growth in concrete by means of fracture mechanics and finite elements. Pergamon, 1976. https://doi.org/10.1016/0008-8846(76)90007-7.

[25] LS-DYNA. Keyword user's manual 2018.

[26] G.D. Quinn, Fractography of Ceramics and Glasses, National Institute of Standards and Technology, Washington, DC, 2016.

[27] G. Hu, J.T. Harris, Z. Tang, J.C. Mauro, Dynamic fracturing of strengthened glass under biaxial tensile loading, J. Non Cryst. Solids 405 (2014) 153–158, https://doi.org/10.1016/j.jnoncrysol.2014.09.007.